METHODS AND APPLICATIONS OF ANALYSIS.
Vol. 29, No. 1, pp. 149–160, March 2022
© 2022 International Press
005

LONG-TIME SIMULATIONS OF ROGUE WAVE SOLUTIONS IN THE NONLINEAR SCHRÖDINGER EQUATION*

CHENXI ZHENG† AND SHAOQIANG TANG‡

Dedicated to Professor Ling Hsiao on the occasion of her 80^{th} birthday

Abstract. Although several short-time simulations have been reported nicely reproducing rogue wave solutions in the nonlinear Schrödinger equation, rogue wave solutions are linearly unstable as shown by theoretical studies. In the present work, we perform long-time simulations for two kinds of rogue wave solutions, namely, the Akhmediev breather and Peregrine soliton. Numerical evidences demonstrate that spurious oscillations that emerge in the central domain in both simulations arise from round-off error and evolve under the mechanism of modulational instability. For the periodic approximation of the Peregrine soliton, the modulational instability also gives rise to additional oscillations on the boundary. We obtain a fitting formula to forecast the time when the boundary oscillations occur. Our simulation results show that a clean and faithful long-time reproduction of rogue wave solutions would be difficult because of the modulational instability.

Key words. Nonlinear Schrödinger equation, modulational instability, numerical simulation, rogue wave.

Mathematics Subject Classification. 76B15, 65N12.

1. Introduction.

Rogue wave is a striking phenomenon that appears from nowhere and disappears without a trace. It was originally identified in oceanography as a wave whose height is bigger than twice the significant wave height. Then it was extended to nonlinear fiber optics, plasmas, Bose-Einstein condensates, etc. [1, 2, 3, 4]. In these fields, the nonlinear Schrödinger equation and its variants are well known models for nonlinear waves.

Rogue wave solutions of the nonlinear Schrödinger equation include the Peregrine soliton [5], Kuznetsov-Ma breather [6, 7] and Akhmediev breather [8]. The Kuznetsov-Ma breather is spatially local and temporally periodic, whereas the Akhmediev breather is spatially periodic and temporally local. The Peregrine soliton is local in both space and time, and can be viewed as the limit of the Kuznetsov-Ma breather or Akhmediev breather. These solutions have been observed experimentally in hydrodynamics [9], plasma physics [10] and nonlinear optics [1]. For more discussions, see [11, 12] and references therein.

The modulational instability, i.e., the instability subject to long wave perturbations, is one of the most ubiquitous phenomena in nonlinear science. When the ground state is a constant wave, such instability is well understood, and plays a pivotal role in the emergence of rogue waves. However, if the ground state is a rogue wave instead, the modulational instability is an open question. Some recent studies showed that the modulational instability may cause the difficulty to simulations. By the Floquet analysis and direct numerical simulations, multiple unstable modes of the ground state were demonstrated to be enhanced in the Kuznetsov-Ma breather [13]. This means that the long-time numerical reproduction of Kuznetsov-Ma breather is difficult. In [14], the authors studied the instantaneous stability of the Akhmediev breather and

*Received May 23, 2020; accepted for publication September 16, 2020.

†HEDPS and LTCS, College of Engineering, Peking University, Beijing 100871, China (zhengchenxi@pku.edu.cn).

‡Corresponding author. HEDPS and LTCS, College of Engineering, Peking University, Beijing 100871, China (maotang@pku.edu.cn).

Peregrine soliton at different time. The instantaneous dispersion relation is the same as that for constant wave ground state except for several wave numbers. As the trivial constant wave solution is unstable, so are the Akhmediev breather or Peregrine soliton expected. Moreover, theoretical studies showed that the Peregrine soliton is orbitally unstable in the family of solitons indexed by a spectral parameter [15]. On the other hand, we notice that the simulations of the Peregrine soliton with periodic boundary condition performed in [16, 17, 18] agreed well with the analytical solution, where the computational time domains were no bigger than $[-2, 2]$, with the rogue wave peak set at $(x, t) = (0, 0)$. The seemingly inconsistency of theoretical and numerical results motivates our exploration to the numerical stability for the Peregrine soliton in long-time simulations.

By long-time simulations with a truncated Peregrine soliton initial profile and periodic boundary condition, we discover that spurious oscillations occur both in the central domain and on the numerical boundary. Since the Akhmediev breather approaches the Peregrine soliton in the limit of infinite period, we first analyze the Akhmediev breather simulations to exclude the effect of boundary condition, and focus on spurious oscillations in the central domain. As expected, the modulational instability is confirmed to be responsible for these spurious oscillations. Gaining an understanding of the Akhmediev breather simulations, we explore the Peregrine soliton. The spurious oscillations in the central domain are found to be the same as in the Akhmediev breather. On the other hand, the spurious oscillations on the boundary arise from the spatially periodic approximation, which turn out to be also induced by the modulational instability. As a conclusion, the modulational instability makes it difficult to reproduce either Akhmediev breather or Peregrine soliton cleanly and faithfully in long-time simulations.

The rest of the paper is organized as follows. In Section 2, we sketch some theoretical results of rogue wave solutions, the modulational instability and numerical method adopted in our simulations. In Section 3, we perform simulations of the Akhmediev breather and demonstrate that the modulational instability causes spurious oscillations in the central domain. In Section 4, simulations are explored to analyze the instability in the central domain and on the numerical boundary for the Peregrine soliton. We make some concluding remarks in Section 5.

2. Preliminaries. In this section, we briefly introduce rogue wave solutions and the modulational instability in the nonlinear Schrödinger equation. We also introduce the numerical scheme adopted in this study.

2.1. Rogue wave solutions of the nonlinear Schrödinger equation. The focusing nonlinear Schrödinger equation reads

$$iu_t + \frac{1}{2}u_{xx} + |u|^2 u = 0, \tag{1}$$

where the modulus of the complex variable $u(x, t)$ describes the modulation of a carrier wave in the water waves, or the mass density in quantum mechanics.

The Akhmediev breather solution of (1) takes the form of

$$u_{AB}(x, t; W) = \frac{(1 - 4a)\cosh(bt) + \sqrt{2a}\cos(\Omega x) + ib\sinh bt}{\sqrt{2a}\cos(\Omega x) - \cosh(bt)} e^{it}, \tag{2}$$

where W is the spatial period, $\Omega = 2\pi/W$, $a = (1 - \Omega^4/4)/2$ and $b = \sqrt{8a(1 - 2a)}$.

When the spatial period tends to infinity, it approaches the Peregrine soliton solution

$$u_{PS}(x,t) = \Big[1 - \frac{4(1+2it)}{1+4x^2+4t^2}\Big]e^{it}. \tag{3}$$

Moreover, both the Akhmediev breather and Peregrine soliton solution converge to the constant wave solution $u_{CW}(x,t) = e^{it}$ when $|t|$ tends to infinity.

As is well known, the nonlinear Schrödinger equation is integrable, and possesses infinite many conservation laws [19]. In quantum mechanics, some conserved quantities have significant physical meanings, such as the mass

$$M = \int_{-\infty}^{\infty} |u|^2 \mathrm{d}x, \tag{4}$$

and the energy

$$E = \int_{-\infty}^{\infty} (|u_x|^2 - |u|^4) \mathrm{d}x. \tag{5}$$

We use these two conserved quantities to validate the numerical algorithm in our study. In another word, we calculate the maximal relative errors

$$\Delta_M = \max_{t\in[t_0,t_e]} \Big|\frac{M(t)}{M(t_0)} - 1\Big|, \tag{6}$$

$$\Delta_E = \max_{t\in[t_0,t_e]} \Big|\frac{E(t)}{E(t_0)} - 1\Big|, \tag{7}$$

where $[t_0, t_e]$ is the time domain of a simulation.

2.2. Modulational instability. The modulational instability refers to that subject to long wave perturbation. It has been studied since the 1960s [20]. The instability depends on the ground state in general.

Now we briefly introduce the modulational instability for the constant wave solution $u_{CW}(x,t) = e^{it}$. We substitute a perturbed solution in the form of

$$u(x,t) = (1 + \epsilon(x,t))e^{it} \tag{8}$$

into (1), where $\epsilon(x,t)$ is a small perturbation. Linearizing about ϵ, we get

$$i\epsilon_t + \frac{1}{2}\epsilon_{xx} + \epsilon + \epsilon^* = 0, \tag{9}$$

where ϵ^* is the complex conjugate of ϵ. Each mode of (9) takes the form of

$$\epsilon(x,t) = A_+(k)e^{ikx+\lambda t} + A_-(k)e^{-ikx-\lambda t}, \tag{10}$$

where $A_-(k)$ and $A_+(k)$ are the amplitudes, k is the spatial wave number and λ is the growth rate. From (9), one obtains the dispersion relation

$$\lambda(k) = \pm\frac{k\sqrt{4-k^2}}{2}. \tag{11}$$

For k smaller than 2, the perturbation grows exponentially at the rate $k\sqrt{4-k^2}/2$. The Fourier mode of wave number $k = \sqrt{2}$ grows fastest at the rate 1.

For the Akhmediev breather as the ground state, the modulational instability is hard to study because the ground state $u_{AB}(x,t;W)$ changes along with time. Recent study explored the transient growth rate at different time [14]. More precisely, consider a perturbed solution in the form of

$$u(x,t) = u_{AB}(x,t;W) + \epsilon'(x,t).$$

It was pointed out that the transient dispersion relation at a fixed time is (11) again except for several wave numbers. When the time is far away from 0, $\epsilon'(x,t)$ asymptotically share exactly the same dispersion relation (11) with $\epsilon(x,t)$. The transient dispersion relation offers a glimpse of the numerical instability for long-time Akhmediev breather simulations, which will be illustrated later.

2.3. Numerical method. We consider the initial-boundary value problem of (1) in $(x,t) \in [-W/2, W/2] \times [t_0, t_e]$ with periodic boundary condition and initial data

$$u(x,t_0) = u_0(x), -W/2 \le x \le W/2. \tag{12}$$

Fourier pseudospectral method has been widely used to conduct numerical studies for the nonlinear Schrödinger equation [21, 22]. Over an equidistant grid with M grid points in space and grid size $h = W/M$, with M an even integer, $u(x,t)$ may be represented by a vector $U(t) = [U_1(t), \cdots, U_M(t)]^T = [u(x_1,t), \cdots, u(x_M,t)]^T$, where $x_j = -W/2 + jh (j = 1, \cdots, M)$. By discrete Fourier transform, the amplitude of a Fourier mode at wave number $k_m = 2\pi(m-1)/M (m = 1, \cdots, M)$ is

$$\hat{U}_m(t) = \frac{1}{M} \sum_{j=1}^{M} U_j(t) e^{-ix_j k_m}. \tag{13}$$

We denote the vector $\hat{U}(t) = [\hat{U}_1(t), , \cdots, \hat{U}_M(t)]^T = \mathcal{F}[U(t)]$.

Conversely, the inverse transform $U(t) = \mathcal{F}^{-1}[\hat{U}(t)]$ with

$$U_j(t) = \sum_{m=1}^{M} \hat{U}_m(t) e^{ik_m x_j}, j = 1, \cdots, M. \tag{14}$$

With a bit abuse of notation, we also denote $\hat{U}(t) = \mathcal{F}[u(x,t)]$.

Fourier transform of (1) gives ordinary differential equations

$$\hat{U}_t = -A\hat{U} + F(\hat{U}), \tag{15}$$

where $A = \dfrac{i}{2} * \mathrm{diag}(k_1^2, k_2^2, \cdots, k_M^2)$ and $F(\hat{U}(t)) = \mathcal{F}\big[|u(x,t)|^2 u(x,t)\big]$. Since the condition number of A is M^2, (15) is a stiff system. To overcome the stiffness, we adopt an exponential time differencing scheme with a fourth order Runge-Kutta type method (ETDRK4) developed by Cox and Matthews [23]:

$$\begin{aligned}
a_n &= e^{-A\Delta t/2}\hat{U}(n\Delta t) - A^{-1}(e^{-A\Delta t/2} - I)F(\hat{U}(n\Delta t)),\\
b_n &= e^{-A\Delta t/2}\hat{U}(n\Delta t) - A^{-1}(e^{-A\Delta t/2} - I)F(a_n),\\
c_n &= e^{-A\Delta t/2}\hat{U}(n\Delta t) - A^{-1}(e^{-A\Delta t/2} - I)\left[2F(b_n) - F(\hat{U}(n\Delta t))\right],\\
\hat{U}\left((n+1)\Delta t\right) &= e^{-A\Delta t}\hat{U}(n\Delta t) - A^{-3}\Delta t^{-2}\Big\{\big[-4 + A\Delta t\\
&\quad + e^{-A\Delta t}(4 + 3A\Delta t + \Delta t^2 A^2)\big]F(\hat{U}(n\Delta t))\\
&\quad + 2\big[2 - A\Delta t + e^{-A\Delta t}(-2 - \Delta t A)\big]\big[F(a_n) + F(b_n)\big]\\
&\quad + \big[-4 + 3A\Delta t - A^2\Delta t^2 + e^{-A\Delta t}(4 + A\Delta t)\big]F(c_n)\Big\},
\end{aligned}$$

where Δt is the time step.

In all our simulations, we take a grid size $h = 200/4096$ and a time step $\Delta t = 1 \times 10^{-4}$ in this article. We have also tried other choices, and the phenomena remain the same.

The ETDRK4 method conserves the mass and energy of the nonlinear Schrödinger equation, which we shall illustrate with the maximal relative errors afterwards.

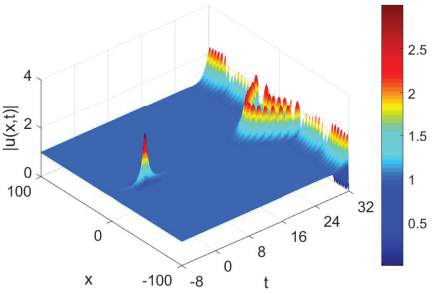

Fig. 1: *Simulation result of the Akhmediev breather:* $AB(200, -8)$

3. Numerical simulations of the Akhmediev breather. We perform numerical simulations of the Akhmediev breather in one spatial period. In order to explore long-time behavior, we terminate the simulation till $t_e = 32$. For convenience, we denote $AB(W, t_0)$ as the numerical simulation result in $(x, t) \in [-W/2, W/2] \times [t_0, 32]$ with initial data

$$u_0(x) = u_{AB}(x, t_0; W), \ x \in [-W/2, W/2]$$

and periodic boundary condition. The snapshot of $AB(200, -8)$ is shown in Fig. 1, which correctly reproduces the peak of the Akhmediev breather solution at $(x, t) = (0, 0)$. However, it does not agree with the Akhmediev breather afterwards. Spurious oscillations arise after the peak, and propagate from the center to both sides. The maximal relative error of mass Δ_M is 9.59×10^{-11}, and that of energy Δ_E is 2.04×10^{-10}. This confirms the conservation laws at discrete level.

Now we demonstrate that the spurious oscillations are due to the modulational instability. To see this, we check the evolution of deviation by its spectrum $A(t) = [A_1(t), \cdots, A_M(t)]^T = \mathcal{F}\big[u(x,t) - u_{AB}(x,t;W)\big]$. The amplitude of the spectrum is symmetric about $k_{M/2}$. So we only show the left half.

Noticing that the spurious oscillations appear prominent at around $t = 22$ in Fig. 1, we plot $\big\{\big(k_m, |A_m(22)|\big)\big|m = 1, \cdots, M/2\big\}$ in Fig. 2(a). $|A_m(22)|$ reaches the local maximum at $m = 46$ and $k_{46} = 1.414$, consistent with the prediction of $k = \sqrt{2} \approx 1.414$ in the modulational instability analysis. Since the round-off error is of the magnitude 10^{-17} in double precision format, we claim that the oscillation of $|A_m(22)|$ near this magnitude is a numerical phenomenon. This also holds true for later spectra.

For convenience, we denote $A^{\sqrt{2}}(t)$ as the amplitude of the Fourier mode at the wave number closest to $\sqrt{2}$. Here $A^{\sqrt{2}}(t) = A_{46}(t)$ is displayed in Fig. 2(b). To make comparison, the spectrum of the exact Akhmediev breather $\hat{u}_{AB}(t) = [\hat{u}_{AB,1}(t), \cdots, \hat{u}_{AB,M}(t)]^T = \mathcal{F}\big[u_{AB}(x,t;W)\big]$ is also shown. $|A^{\sqrt{2}}(t)|$ is much smaller

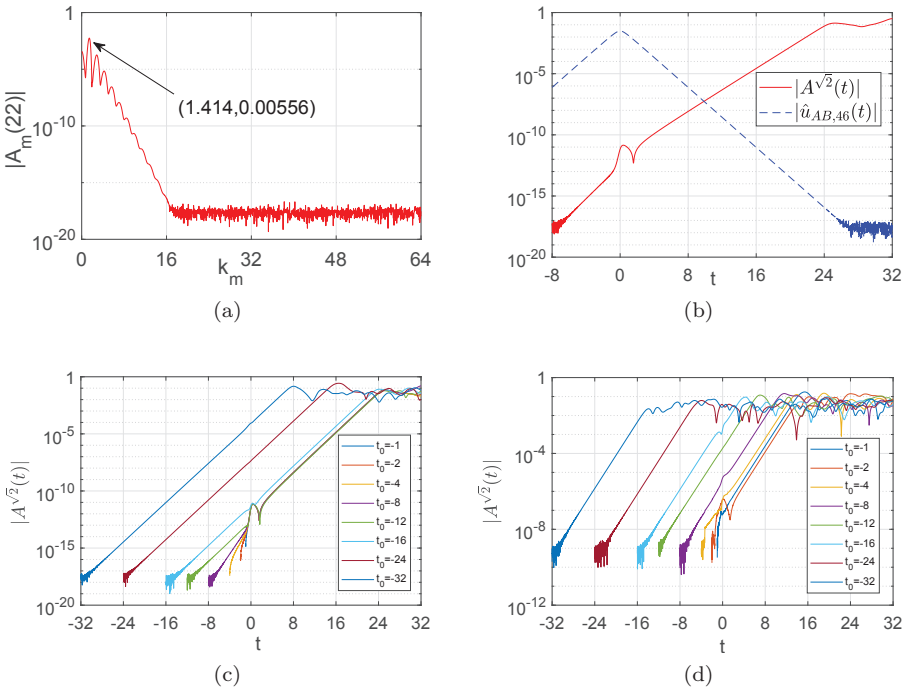

Fig. 2: *Spectrum analysis of AB(200,-8): (a) $|A_m(22)|$; (b) solid line for $|A_{46}(t)|$ and dash line for $|\hat{u}_{AB,46}(t)|$; (c) $|A_{46}(t)|$ with different starting time t_0 ; (d) $|A_{46}(t)|$ with different starting time t_0 and single precision calculations.*

than $|\hat{u}_{AB,46}(t)|$ in the early stage. As time elapses, $|A^{\sqrt{2}}(t)|$ becomes larger than $|\hat{u}_{AB,46}(t)|$, thereby contaminates simulation results. The growth rate of $|A^{\sqrt{2}}(t)|$ constantly changes near the peak because of the strong nonlinear effect. After that, the growth rate becomes 1.013, consistent with the theoretically predicted growth rate 1.

By comparing the simulation results with different t_0 in Fig. 2(c), the growth rate maintains at 1 all the time for simulation started even earlier. In all cases, $|A^{\sqrt{2}}(t)|$ grows from the round-off error of the magnitude 10^{-17}. In comparison, by single precision calculations as shown in Fig. 2(d), the deviation comes from the error of a bigger magnitude 10^{-9} instead, and at the rate of 1 as well. When the disturbance saturates, it produces the spurious oscillations in the central domain.

In summary, round-off errors initiate spurious oscillations, while the modulational instability is the underlying mechanism for the persistent growth. Analysis on the deviation shows that the Fourier mode at $k_{46} = 1.414$ is most noticeable, consistent with theoretical prediction. Simulations with different initial time show that $|A^{\sqrt{2}}(t)|$ grows from the round-off error and at the rate about 1. Therefore, it is the modulational instability that causes difficulty in clean and faithful numerical reproduction of the Akhmediev breather over a long time.

4. Numerical simulations of the Peregrine soliton. The Peregrine soliton is the infinite period limit of the Akhmediev breather. Moreover, the fairly small

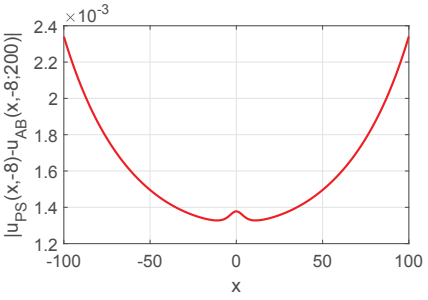

Fig. 3: *Difference between* $u_{PS}(x,-8)$ *and* $u_{AB}(x,-8;200)$.

difference between $u_{PS}(x,-8)$ and $u_{AB}(x,-8;200)$ is shown in Fig. 3, bigger on the boundary. This predicts the appearance of spurious oscillations in the central domain for the simulations of the Peregrine soliton. While the Peregrine soliton is defined on the unbounded domain, here we only perform numerical simulations over a truncated domain. More precisely, we denote $\widetilde{PS}(W,t_0)$ as the simulation result in $[-W/2,W/2]\times[t_0,32]$ with the truncated initial data

$$u_0(x)=u_{PS}(x,t_0),\ x\in[-W/2,W/2]$$

and periodic boundary condition. As an example, $\widetilde{PS}(200,-8)$ is shown in Fig. 4. It is remarkable that the spurious oscillations arise not only in the central domain, but also on the boundary. In this simulation, the maximal relative error of mass Δ_M is 1.04×10^{-10}, and that of energy Δ_E is 2.59×10^{-10}, indicating that the mass and energy are conserved at discrete level.

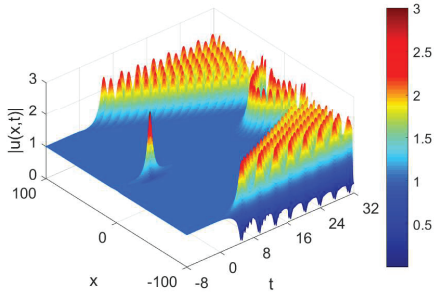

Fig. 4: *Simulation result of the Peregrine soliton:* $\widetilde{PS}(200,-8)$.

As expected before, spurious oscillations appear in the central domain. In Fig. 5, we compare $AB(200,-8)$ and $\widetilde{PS}(200,-8)$ in this domain at $t=24$. They coincide in both real and image parts. More careful study shows that the difference is smaller than 1×10^{-2}. Therefore, in the Peregrine soliton simulation, spurious oscillations in the central domain also arise from the round-off error and grow due to the modulational instability.

Next, we study the spurious oscillations on the boundary. With the periodic boundary condition, $\widetilde{PS}(W,t_0)$ can be regarded as the simulation result with the

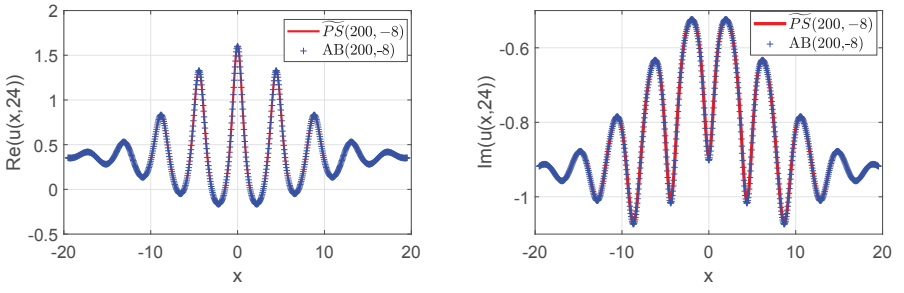

Fig. 5: *The comparison of* $AB(200,-8)$ *and* $\widetilde{PS}(200,-8)$ *at t=24: (a) the real part; (b) the imaginary part.*

initial data of a perturbed Akhmediev breather

$$\begin{aligned} u_0(x) =& u_{PS}(x,t_0) \\ =& u_{AB}(x,t_0;W) + [u_{PS}(x,t_0) - u_{AB}(x,t_0;W)],\ x \in [-W/2, W/2]. \end{aligned}$$

The Akhmediev breather part satisfies the boundary condition naturally. We claim that the perturbation part evolves into the oscillation on the boundary because of the modulational instability.

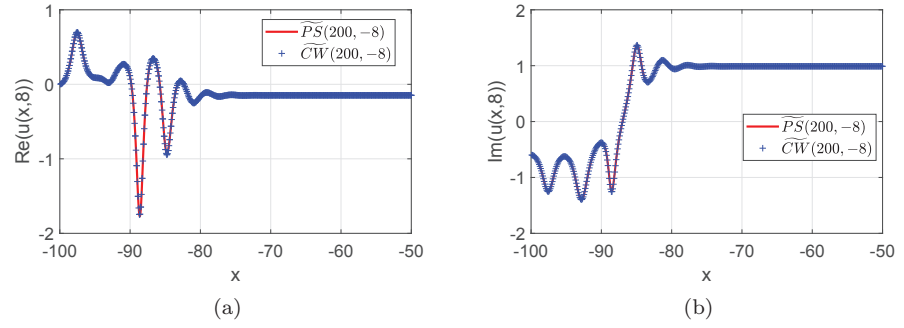

Fig. 6: *Comparison of* $\widetilde{CW}(200,-8)$ *and* $\widetilde{PS}(200,-8)$ *near the boundary at* $t = 8$*: (a) The real part; (b) the imaginary part.*

To verify this, we explore the evolution of this perturbation. Since close to the boundary $u(x,t)$ is almost the same as the constant wave solution, for which the modulational instability is theoretically clear, we perform simulation in $[-W/2, W/2] \times [t_0, 32]$ with periodic boundary condition and perturbed initial data

$$u_0(x) = e^{it_0} + [u_{PS}(x,t_0) - u_{AB}(x,t_0;W)], x \in [-W/2, W/2].$$

The simulation result is denoted by $\widetilde{CW}(W,t_0)$. A comparison of $\widetilde{CW}(200,-8)$ and $\widetilde{PS}(200,-8)$ near the boundary at $t = 8$ is made. See Fig. 6. The oscillations on the boundary agree very well.

With the knowledge of the modulational instability for the constant wave, we realize that $A^{\sqrt{2}}(t)$ is important. We mark the time t_{bd} when $|u(100,t)|$ reaches 0.99. In order to find the influence of the Fourier mode at $k=\sqrt{2}$ quantitatively, we list the time $t_{bd}-t_0$ and $\ln|A^{\sqrt{2}}(t_0)|$ with different starting time t_0 and width W in Table 1. See Fig. 7. By linear fitting, we obtain a relationship between $t_{bd}-t_0$ and $\ln|A^{\sqrt{2}}(t_0)|$:

$$\ln|A^{\sqrt{2}}(t_0)| = -1.23(t_{bd}-t_0) - 5.05, \tag{16}$$

that is,

$$|A^{\sqrt{2}}(t_0)|e^{1.23(t_{bd}-t_0)} = 0.0064. \tag{17}$$

We speculate that $\ln|A^{\sqrt{2}}(t_0)|$ plays an important role in the generation of the spurious oscillations on the boundary.

We also remark that the growth rate in the linear fitting is bigger than 1, which is inconsistent with the modulational instability analysis. This will be explored in the future.

W	200	200	200	200	400	600	800
t_0	-16	-12	-8	-4	-8	-8	-8
t_{bd}	-8.65	-4.35	0.09	4.91	2.28	3.56	4.46
$t_{bd}-t_0$	7.35	7.65	8.09	8.91	10.28	11.56	12.46
$\lvert A^{\sqrt{2}}(t_0)\rvert$	-14.31	-14.58	-14.97	-15.67	-17.72	-19.35	-20.49

Table 1: *Time $t_{bd}-t_0$ and amplitude $|A^{\sqrt{2}}(t_0)|$ with different starting time t_0 and width W.*

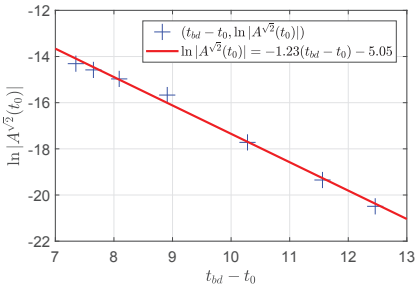

Fig. 7: *Numerical data of $(t_{bd}-t_0, |A^{\sqrt{2}}(t_0)|)$ and the fitting curve.*

In summary, it is the modulational instability that produces spurious oscillations in the Peregrine soliton simulations as well. Similar to the Akhmediev breather, the spurious oscillations in the central domain emerge after the peak and are induced by the modulational instability. Besides, under periodic boundary condition, the modulational instability also causes spurious oscillations on the boundary, which propagate to the interior domain and contaminate the central domain over time. We obtain a fitting formula to forecast when the boundary oscillations occur. It suggests that the Fourier mode $A^{\sqrt{2}}(t)$ plays a dominant role. We conclude that spurious oscillations induced by the modulational instability in the central domain and on the boundary

make it difficult to reproduce numerically the Peregrine soliton clean and faithfully in a long-time simulation.

5. Conclusion. In this work, using a mass and energy conserved numerical method ETDRK4, we perform simulations under spatially periodic boundary condition for both the Akhmediev breather and Peregrine soliton. Spurious oscillations show up in the central domain. For the periodic approximation of the Peregrine soliton, additional oscillations appear on the boundary. By careful spectral and dynamics analysis, we demonstrate the modulational instability to be the underlying mechanism to amplify the deviation from exact rogue wave solutions, responsible for the spurious oscillations both in the central domain and on the numerical boundary. As a consequence, clean and faithful reproduction of the rogue wave solution in a long-time simulation would be difficult, if possible. In [24], stabilization was suggested by switching the focusing nonlinear Schrödinger equation into the defocusing one.

In the future, it would be interesting to design suitable numerical boundary treatments for finite domain simulation of the Peregrine soliton, with the spurious oscillation on the boundary eliminated. It is more challenging to eliminate spurious oscillations in the central domain, which would require to devise a numerical algorithm that confines in a subspace of functions free of the oscillations induced by the modulational instability.

Although only simulations by ETDRK4 method are reported here, we have applied other numerical methods, such as Crank-Nicolson finite difference method and time splitting pseudospectral method. Similar phenomena are observed. These suggest that the nonlinear Schröodinger equation admits solutions with oscillations. That is, there are some solutions displaying totally different behaviors near the exact rogue wave solutions. Enlightening study showed that the Peregrine soliton is unstable in a family of scaled Peregrine soliton type solutions [15]. However, it needs further studies to clarify the unstable perturbation and to describe their evolution.

Acknowledgements. This work is supported in part by the NSFC under grant numbers 11832001, 11988102, and 11890681.

We thank Mr. Hanqing Yin and the anonymous reviewers for stimulating discussions.

REFERENCES

[1] B. Kibler, J. Fatome, C. Finot, G. Millot, F. Dias, G. Genty, N. Akhmediev, and J. M. Dudley, *The Peregrine soliton in nonlinear fibre optics*, Nature Physics, 6:10 (2010), pp. 790–795.

[2] N. Akhmediev, J. M. Dudley, D. R. Solli, and S. Turitsyn, *Recent progress in investigating optical rogue waves*, Journal of Optics, 15:6 (2013), 060201.

[3] N. Akhmediev, B. Kibler, F. Baronio, M. Belić, W. P. Zhong, Y. Q. Zhang, W. Chang, J. M. Soto-Crespo, P. Vouzas, P. Grelu, et al., *Roadmap on optical rogue waves and extreme events*, Journal of Optics, 18:6 (2016), 063001.

[4] C. Kharif and E. Pelinovsky, *Physical mechanisms of the rogue wave phenomenon*, European Journal of Mechanics-B/Fluids, 22:6 (2003), pp. 603–634.

[5] D. Peregrine, *Water waves, nonlinear Schrödinger equations and their solutions*, The ANZIAM Journal, 25:1 (1983), pp. 16–43.

[6] E. A. Kuznetsov, *Solitons in a parametrically unstable plasma*, Akademiia Nauk SSSR Doklady, 236 (1977), pp. 575–577.

[7] Y. C. Ma, *The perturbed plane-wave solutions of the cubic Schrödinger equation*, Studies in Applied Mathematics, 60:1 (1979), pp. 43–58.

[8] N. Akhmediev and V. I. Korneev, *Modulation instability and periodic solutions of the nonlinear Schrödinger equation*, Theoretical and Mathematical Physics, 69:2 (1986), pp. 1089–1093.
[9] A. Chabchoub, N. P. Hoffmann, and N. Akhmediev, *Rogue wave observation in a water wave tank*, Physical Review Letters, 106:20 (2011), 204502.
[10] H. Bailung, S. K. Sharma, and Y. Nakamura, *Observation of Peregrine solitons in a multicomponent plasma with negative ions*, Physical Review Letters, 107:25 (2011), 255005.
[11] J. M. Dudley, F. Dias, M. Erkintalo, and G. Genty, *Instabilities, breathers and rogue waves in optics*, Nature Photonics, 8:10 (2014), pp. 755–764.
[12] G. Biondini and E. Fagerstrom, *The integrable nature of modulational instability*, SIAM Journal on Applied Mathematics, 75:1 (2015), pp.136–163.
[13] J. Cuevas-Maraver, P. G. Kevrekidis, D. J. Frantzeskakis, N. I. Karachalios, M. Haragus, and G. James, *Floquet analysis of Kuznetsov-Ma breathers: A path towards spectral stability of rogue waves*, 96:1 (2017), 012202.
[14] U. Al-Khawaja, H. Bahlouli, M. Asad-uz-zaman, and S. M. Al-Marzoug, *Modulational instability analysis of the Peregrine soliton*, Communications in Nonlinear Science and Numerical Simulation, 19:8 (2014), pp. 2706–2714.
[15] R. A. Van Gorder, *Orbital instability of the Peregrine soliton*, Journal of the Physical Society of Japan, 83:5 (2014), 054005.
[16] S. A. El-Tantawy and T. Aboelenen, *Simulation study of planar and nonplanar super rogue waves in an electronegative plasma: Local discontinuous Galerkin method*, Physics of Plasmas, 24:5 (2017), 052118.
[17] W. J. Cai, Y. S. Wang, and Y. Z. Song, *Numerical simulation of rogue waves by the local discontinuous Galerkin method*, Chinese Physics Letters, 31:4 (2014), 040201.
[18] M. Birem and C. Klein, *Multidomain spectral method for Schrödinger equations*, Advances in Computational Mathematics, 42:2 (2016), pp. 395–423.
[19] J. I. Ramos and F. R. Villatoro, *Classical forces on solitons in finite and infinite nonlinear planar waveguides*, Microwave and Optical Technology Letters, 7:13 (1994), pp. 620 –625.
[20] T. B. Benjamin and J. E. Feir, *The disintegration of wave trains on deep water Part 1. Theory*, Journal of Fluid Mechanics, 27:3 (1967), pp. 417–430.
[21] B. Fornberg, *A Practical Guide to Pseudospectral Methods*, Cambridge University Press, Cambridge, 1998.
[22] B. Fornberg and D. M. Sloan, *A review of pseudospectral methods for solving partial differential equations*, Acta Numerica, 3 (1994), pp. 203–267.
[23] S. Cox and P. Matthews, *Exponential time differencing for stiff systems*, Journal of Computational Physics, 176:2 (2002), pp. 430–455.
[24] J. Cuevas-Maraver, B. A. Malomed, P. G. Kevrekidis, and D. J. Frantzeskakis, *Stabilization of the Peregrine soliton and Kuznetsov–Ma breathers by means of nonlinearity and dispersion management*, Physics Letters A, 382:14 (2018), pp. 968–972.